



# Aberration-free pupil steering Maxwellian display with wide-view broadband polarization converters

Jianghao Xiong, SID Student Members<sup>1</sup>  | Yannanqi Li, SID Student Members<sup>1</sup> | Kun Li, SID Members<sup>2</sup> | Shin-Tson Wu, SID Fellow<sup>1</sup> 

<sup>1</sup>College of Optics and Photonics, University of Central Florida, Orlando, Florida, USA

<sup>2</sup>Goertek Electronics, Santa Clara, California, USA

## Correspondence

Shin-Tson Wu, College of Optics and Photonics, University of Central Florida, Orlando, FL 32816, USA.  
Email: swu@creol.ucf.edu

## Funding information

GoerTek Electronics

## Abstract

A see-through Maxwellian display with aberration-free pupil steering is proposed and experimentally demonstrated. The system uses a polarization-dependent off-axis lens coupler set fabricated with cholesteric liquid crystal. Electrically addressable polarization converters are used to switch among pupils. A wide-view broadband polarization converter is designed accordingly.

## KEYWORDS

augmented reality, cholesteric liquid crystal, Maxwellian display, pupil steering

## 1 | INTRODUCTION

Augmented reality (AR) aims to provide a seamless experience of blending virtual digital images with real environment.<sup>1–4</sup> To build an AR system with decent viewing experience, numerous parameters should be considered, including field of view (FOV), eyebox, and image brightness. Traditional optics with refractive and reflective surfaces faces the issue of conserved étendue where there exists a tradeoff between FOV and eyebox. To simultaneously enlarge both FOV and eyebox requires a larger optical system, which compromises the wearing comfort.

Waveguide display<sup>2–4</sup> is a potential solution to overcome this issue. In a waveguide display, the collimated light experiences multiple total internal reflections (TIRs) and gets out-coupled each time it encounters the out-coupler. With this mechanism, the étendue is no longer conserved because each out-coupling increases the eyebox size. However, the enlarged eyebox also has a disadvantage of compromised light efficiency and therefore image brightness. To increase the light efficiency in the out-coupling process requires a dynamic control of efficiency of each out-coupling, which is very challenging, if not impossible.

Another promising architecture is Maxwellian display or retinal scanning display.<sup>5–15</sup> The basic concept of Maxwellian display is to focus the spatially modulated, collimated light onto the viewer's pupil and form images on retina, as Figure 1A shows. Because all the imaging light is directed onto the viewer's eye, the light efficiency of a Maxwellian display is nearly 100% in theory. However, because the viewing point is smaller than the pupil diameter, a slight eye movement would miss the image, which is deemed as a major disadvantage of Maxwellian display.

To solve the issue of small eyebox, pupil duplication and steering have been proposed. In pupil duplication, the viewing point is duplicated through splitting the incident image rays<sup>7,9</sup> or multiplexing holograms in the coupler,<sup>10,13,16</sup> as depicted in Figure 1B,C. Although the eyebox can be expanded accordingly, the efficiency decreases. Another issue is the possible ghost image if more than one viewing point enters eye pupil. Pupil steering<sup>5,8,11–13,15,17</sup> has a much higher light efficiency. However, all previous works are based on changing the incident angle of image rays to shift the focus point, as shown in Figure 1D. This approach works well only when the steering range is small. As the steering range increases, serious aberrations like coma will start to distort and expand the viewing point. Additionally, the

**FIGURE 1** (A) Schematic plot of a see-through Maxwellian display. Pupil duplication method using (B) grating and (C) multiplexed hologram. (D) Pupil steering method

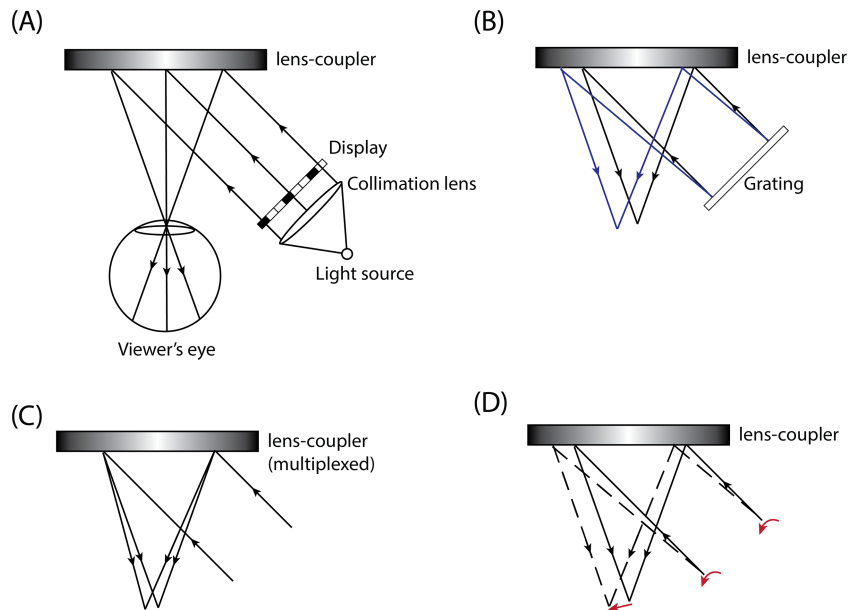
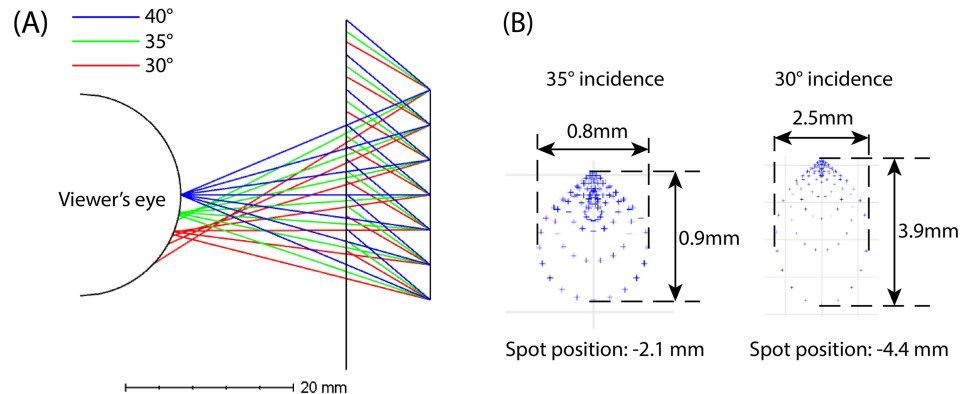


**FIGURE 2** (A) Ray tracing plot of pupil steering. (B) Spot size at different incident angles



tuning of incident ray angle often requires mechanical rotating mirror or backlight modulation system, which complicates the system design.

## 2 | SYSTEM DESIGN

### 2.1 | Pupil steering

Previous pupil steering methods are based on changing the incident angle of image light. Here, we provide a simple analysis of aberration. The simulation is performed in Opticstudio (Zemax). The lens has a diameter of 24 mm and focal length of 30 mm, which corresponds to  $FOV = 43^\circ$ . The off-axis angle is  $40^\circ$ .

To shift the viewing point location, the incident angle is set at  $35^\circ$  and  $30^\circ$ . Because the eye has a near-ball shape, the image plane is set to have radius curvature of 12 mm. Figure 2A shows the ray-tracing result. The

shape of spot indicates that coma is the main attributor of aberration. At  $35^\circ$  incidence, the viewing point shifts by 2.1 mm, and the spot diameter increases to 0.8 mm by 0.9 mm. At  $30^\circ$  incidence, the viewing point further shifts to 4.4 mm, and the spot diameter significantly increases to 2.5 mm by 4.4 mm, which is already comparable with human pupil size. A large spot size means some peripheral rays would not enter eye pupil, which compromises the FOV. Here, we do not use RMS spot size as criteria because in Maxwellian display the peripheral rays also contribute to FOV and should be considered equally. Moreover, a bigger spot size also influences the always-in-focus feature of Maxwellian display. This means when the viewer is looking at a different depth, the image on retina can be distorted.

Our proposed system uses a polarization-dependent lens coupler fabricated through cholesteric liquid crystal (CLC) polarization holography.<sup>18,19</sup> Like traditional CLC, the CLC lens coupler only responds to one circular

polarization and transmits the other. The patterning method of CLC is photoalignment polarization holography that uses two beams with left-handed circular polarization (LCP) and right-handed circular polarization (RCP) to form the spatially varying linear polarization patterns. The CLC in contact with the patterned photoalignment layer then form the tilted helical structure<sup>20</sup> that exhibits strong Bragg diffraction. Detailed operation principles and fabrication methods have been described previously.<sup>20,21</sup>

The system setup and working principle are illustrated in Figure 3. Three CLC lenses and switchable half-wave plates (HWPs) are stacked together. The CLC lenses respond to LCP light. When the incident light has LCP state and HWP1 is in off-state, the incident light passes HWP1 and gets reflected by coupler L1 and focused onto viewpoint P, as shown in Figure 3A. When HWP1 and HWP2 are both turned on, the incident LCP light is firstly converted to RCP and then passes L1 due to the polarization selectivity of CLC. Then, the RCP light encounters HWP2 and is converted to LCP again. The light is then reflected by coupler L2 and focused onto viewpoint Q. It should be noted that the reflected LCP light is firstly converted to RCP again by HWP2. This means the light would pass through L1 and enter viewpoint Q. The incident angle range on HWP2 is determined by the system's FOV. Therefore, a wide-view polarization converter is required. The working principle for the third viewpoint is similar. To keep Figure 3 clear, the light paths for the third viewpoint are not shown. By turning-on HWP1 and HWP3 while turning-off HWP2, the light would be converted to RCP and goes through L1 and L2. Then, it is converted back to LCP by HWP3 and gets coupled by L3 to the third viewpoint. In theory, more viewpoints can be achieved by adding more pairs of CLC lens and polarization converter accordingly.

Because each coupler is recorded individually, in theory, the aberration can be eliminated for each viewpoint if the recording template lens is diffraction limited. Another advantage of the system is its relative simplicity.

Because the pupil steering process occurs in the out-coupler module, no complicated design is needed in the image-generating module. Although stacking multiple couplers together seems to increase the system's volume, the actual thickness of lens coupler and HWP is only about 2  $\mu\text{m}$ . The major thickness comes from the glass substrate. If we use a 0.1-mm-thick glass substrate, then stacking 10 lenses together only leads to a 2-mm-thick final out-coupler.

Here, to build a proof-of-concept system, we use two CLC lenses and a polarization converter. The CLC lenses have opposite handedness. The polarization converter is a simple homogeneous cell with cell gap  $d = 2 \mu\text{m}$  and LC material DIC LC-1 ( $\Delta n = 0.284$ ).

## 2.2 | Wide-view broadband polarization converter

As mentioned earlier, the polarization converter should accommodate a large range of incident angles. Furthermore, if we want to build a full-color display, the polarization converter should also be a broadband device. Compared with the homogeneous cell used in our proof-of-concept demo, twisted nematic (TN) cell exhibits a much wider bandwidth.<sup>22,23</sup> When combined with a wide-view and broadband quarter-wave plate (QWP), it can achieve the desired function. The proposed structure is sketched in Figure 4. Two QWP A-films A1 and A4 and two HWP A-films A2 and A3 are used. The angle between optical axis and  $x$ -axis is  $75^\circ$ ,  $15^\circ$ ,  $-75^\circ$ , and  $-15^\circ$ , respectively, which is similar to a reported structure.<sup>24</sup> We used a  $4 \times 4$  matrix method to simulate the results. In the simulation, the LC material is 5CB. The refractive indices of A-film are  $n_e = 1.5902$  and  $n_o = 1.5866$ . The thickness of the QWP film and HWP film is 38.2 and 76.4  $\mu\text{m}$ , respectively. The cell gap of TN cell is 2.52  $\mu\text{m}$ . The birefringence dispersion of LC<sup>25</sup> is also considered in the simulation.

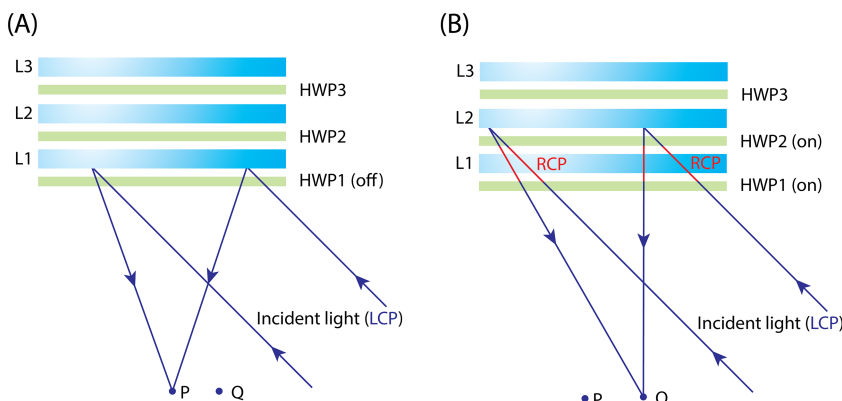


**FIGURE 3** Illustration of the working principle of proposed system. (A) Rays are focused onto viewpoint P. (B) Rays are steered onto viewpoint Q

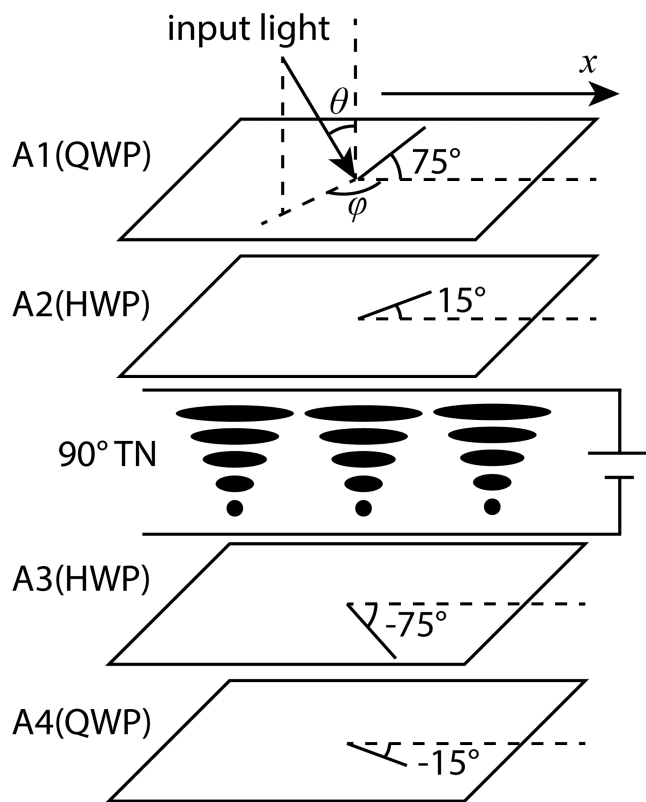


**FIGURE 4** Structure of the proposed wide-view broadband polarization converter

### 3 | RESULTS AND DISCUSSIONS

#### 3.1 | Pupil steering see-through display

We fabricated two CLC lenses with diameter of 24 mm and focal length of 35 mm, as shown in Figure 5A. Then, we used an optical glue NOA65 to laminate the two couplers. A sample photo is shown in Figure 5B. We can see two images of the ceiling light, which indicates two couplers. These two lenses have opposite CLC handedness, which means they respond to opposite circular polarization. A single polarization converter is able to switch between viewpoints, which simplifies our device fabrication. We also measured the polarization response of the lenses. When the incident light ( $\lambda = 457 \text{ nm}$ ) was in the LCP state, its total power was 4.1 mW. The power at focal point was measured to be 2.4 mW for the left-handed CLC lens and 3.6  $\mu\text{W}$  for the right-handed CLC lens. When the incident light was in the RCP state, the power at focal point was 4.0  $\mu\text{W}$  for the left-handed CLC lens and 2.5 mW for the right-handed CLC lens. Therefore, the efficiency of each lens was around 60%. The contrast ratio between two lenses was 625:1 and 667:1 for these two modes, indicating the crosstalk is very small.

A photo of the display system is shown in Figure 5C. The projected laser beam firstly passes through a neutral

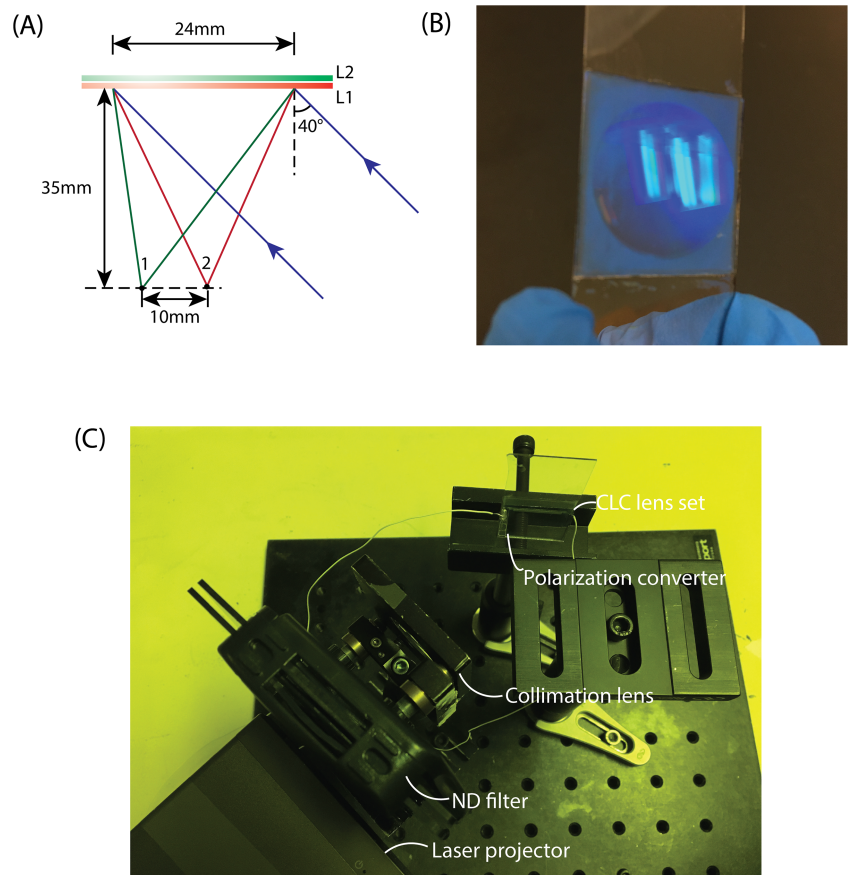


**FIGURE 5** (A) Configuration of the fabricated CLC lenses. (B) Photo of the fabricated CLC lens sample. (C) Photo of the display system. CLC, cholesteric liquid crystal; ND, neutral density

density (ND) filter and a collimation lens. Then, the imaging light encounters the coupler, which consists of the polarization converter and two CLC lenses. The reason for using a ND filter is to prevent overexposure to our camera. Thus, we dim the imaging light to 1/16. This also indicates the high efficiency of our display system, which promises its use even in a bright outdoor environment. We could also remove the ND filter by reducing the display brightness, or fabricate a CLC lens with a lower efficiency.

To mimic human eye, we used a smartphone with a single camera to take the photo. Results are shown in Figure 6A for viewpoint 1 and Figure 6B for viewpoint 2. We can see that the image quality is good for both viewpoints. Notice how the relative position between the image and background is changed when

the viewpoint is switched. Because the CLC lens has little scattering, the background is clear. Also, because the CLC lens can diffract a portion of blue light from environment, the background image appears a little yellowish. This can be alleviated by decreasing the lens efficiency.

The response time of pupil steering is determined by the LC cell, which is about several milliseconds. This is sufficient because the time for human eye moving 10 mm (separation of the viewpoints) is about 50 ms. During experiment, we drove the homogeneous LC cell at a relatively low voltage, and as a result, the switching time is slower.<sup>26</sup> In the proposed wide-view broadband polarization converter using a TN cell, such an on-off switching time could be <10 ms, depending on the cell gap and LC material.

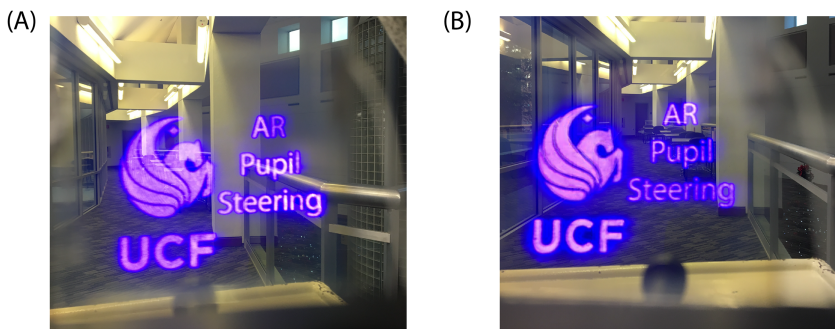


FIGURE 6 Photos of the display system at viewpoint (A) 1 and (B) 2

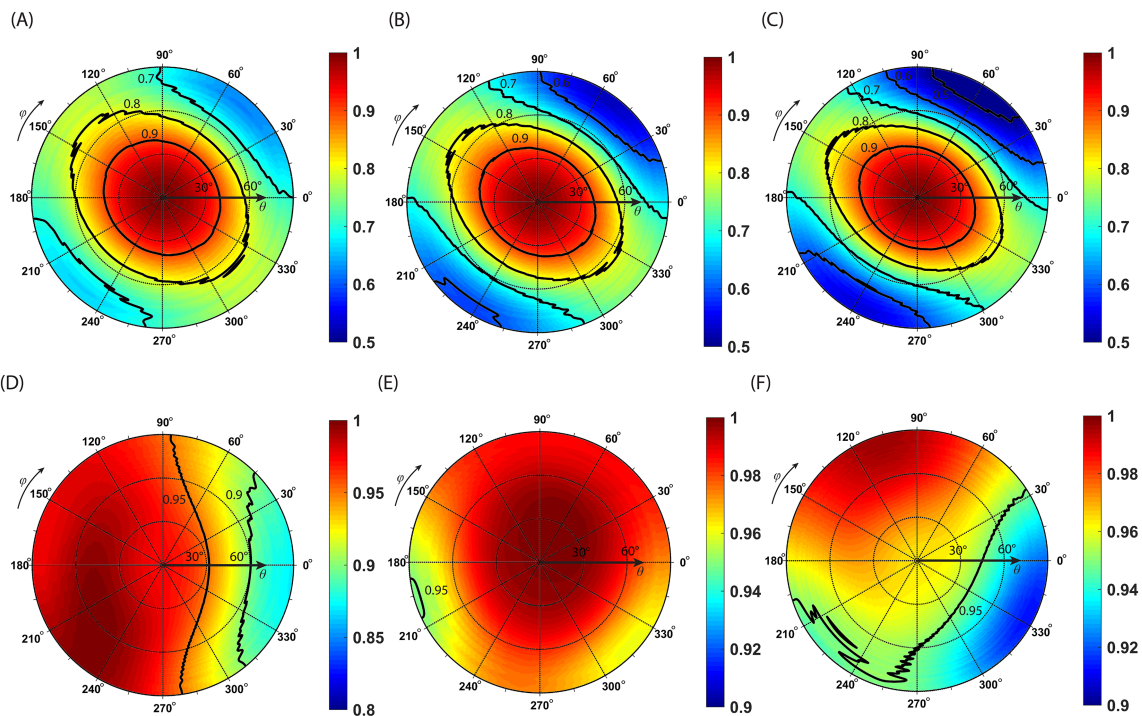


FIGURE 7 Simulated optical efficiency of the wide-view twisted nematic (TN) polarization rotator. Relations between efficiency and incident angles (polar and azimuthal) in voltage-on state for (A) red, (B) green, and (C) blue wavelengths. Efficiency plots in voltage-off state for (D) red, (E) green, and (F) blue wavelengths

### 3.2 | Wide-view broadband polarization converter

A TN cell is a broadband, but not wide-view polarization rotator. Therefore, we need to add wide-view compensation films, as Figure 4 depicts. The simulation results of such a polarization converter are plotted in Figure 7. The input light is RCP light. The efficiency is defined as the LCP (or RCP) proportion of output light. Figure 7A–C shows the voltage-on relations between efficiency and incident angles  $\theta$  (polar) and  $\varphi$  (azimuthal) for red (630 nm), green (532 nm), and blue (465 nm) colors, respectively. Figure 7D–F shows the voltage-off relations. In the voltage-off state, within  $30^\circ$  of incident polar angle, the efficiency generally maintains larger than 90% for RGB wavelengths. This corresponds to a FOV of  $60^\circ$ . In the voltage-on state, the performance is even better. The efficiency is larger than 90% within  $60^\circ$  of incident polar angle, which means a FOV of  $120^\circ$ .

It should be mentioned that in the simulation of voltage-on state, the LC director is assumed to align vertically, and we did not consider the residual phase resulting from the alignment. To compensate for the residual phase of TN cell, a discotic film has been developed.<sup>27</sup>

## 4 | CONCLUSION

We proposed and implemented a see-through Maxwellian display with aberration-free pupil steering. The coupler lenses are recorded individually for each viewpoint. These devices are fabricated from CLC and exhibit distinct polarization selectivity. Polarization converters are sandwiched between lenses to control the light polarization state and therefore determine which coupler to activate. The system has a relatively fast response time and simple architecture. A wide-view and broadband polarization converter using TN cell and broadband QWPs is also proposed. The performance is analyzed with a  $4 \times 4$  matrix method. The efficiency is larger than 90% across the  $60^\circ$  FOV for the RGB wavelengths.

### ACKNOWLEDGMENT

The authors are indebted to GoerTek Electronics for the financial support.

### ORCID

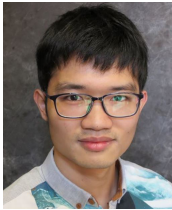
Jianghao Xiong  <https://orcid.org/0000-0002-8122-9936>  
Shin-Tson Wu  <https://orcid.org/0000-0002-0943-0440>

## REFERENCES

1. Cakmakci O, Rolland J. Head-worn displays: a review. *J Disp Technol*. 2006;2:199–216.
2. Kress BC, Chatterjee I. Waveguide combiners for mixed reality headsets: a nanophotonics design perspective. *Nanophotonics*. 2021;10:41–74.
3. Lee Y-H, Zhan T, Wu S-T. Prospects and challenges in augmented reality displays. *Virtual Reality Intell Hardw*. 2019;1:10–20.
4. Zhan T, Yin K, Xiong J, He Z, Wu S-T. Augmented reality and virtual reality displays: perspectives and challenges. *iScience*. 2020;23:101397.
5. Chang C, Cui W, Park J, Gao L. Computational holographic Maxwellian near-eye display with an expanded eyebox. *Sci Rep*. 2019;9:18749.
6. Lee JS, Kim YK, Lee MY, Won YH. Enhanced see-through near-eye display using time-division multiplexing of a Maxwellian-view and holographic display. *Opt Express*. 2019;27:689–701.
7. He Z, Yin K, Fan-Chiang K-H, Wu S-T. Enlarging the eyebox of Maxwellian displays with a customized liquid crystal Damann grating. *Crystals*. 2021;11:195.
8. Hedili MK, Soner B, Ulusoy E, Urey H. Light-efficient augmented reality display with steerable eyebox. *Opt Express*. 2019;27:12572–81.
9. Lin T, Zhan T, Zou J, Fan F, Wu S-T. Maxwellian near-eye display with an expanded eyebox. *Opt Express*. 2020;28:38616–25.
10. Kim S-B, Park J-H. Optical see-through Maxwellian near-to-eye display with an enlarged eyebox. *Opt Lett*. 2018;43:767–70.
11. Jang C, Bang K, Moon S, Kim J, Lee S, Lee B. Retinal 3D: augmented reality near-eye display via pupil-tracked light field projection on retina. *ACM Trans Graph*. 2017;36:190.
12. Ratnam K, Konrad R, Lanman D, Zannoli M. Retinal image quality in near-eye pupil-steered systems. *Opt Express*. 2019;27:38289–311.
13. Yoo C, Chae M, Moon S, Lee B. Retinal projection type lightguide-based near-eye display with switchable viewpoints. *Opt Express*. 2020;28:3116–35.
14. Lee JS, Kim YK, Won YH. Time multiplexing technique of holographic view and Maxwellian view using a liquid lens in the optical see-through head mounted display. *Opt Express*. 2018;26:2149–59.
15. Travis ARL, Chen L, Georgiou A, Chu J, Kollin J. Wedge guides and pupil steering for mixed reality. *J Soc Inf Disp*. 2018;26:526–33.
16. Park J-H, Kim S-B. Optical see-through holographic near-eye-display with eyebox steering and depth of field control. *Opt Express*. 2018;26:27076–88.
17. Jang C, Bang K, Li G, Lee B. Holographic near-eye display with expanded eye-box. *ACM Trans Graph*. 2018;37:195.
18. Xiong J, Yin K, Li K, Wu S-T. Holographic optical elements for augmented reality: principles, present status, and future perspectives. *Adv Photonics Res*. 2021;2:2000049.
19. Yin K, He Z, Wu ST. Reflective polarization volume lens with small f-number and large diffraction angle. *Adv Opt Mater*. 2020;8:2000170.
20. Xiong J, Chen R, Wu S-T. Device simulation of liquid crystal polarization gratings. *Opt Express*. 2019;27:18102–12.

21. Xiong J, Tan G, Zhan T, Wu S-T. Breaking the field-of-view limit in augmented reality with a scanning waveguide display. *OSA Continuum*. 2020;3:2730–40.
22. Wang Q-H, Wu TX, Zhu X, Wu S-T. Achromatic polarization switch using a film-compensated twisted nematic liquid crystal cell. *Liq Cryst*. 2004;31:535–9.
23. Wu TX, Huang Y, Wu S-T. Design optimization of broadband linear polarization converter using twisted nematic liquid crystal. *Jpn J Appl Phys*. 2003;42:L39–41.
24. Ge Z, Jiao M, Lu R, et al. Wide-view and broadband circular polarizers for transmissive liquid crystal displays. *J Disp Technol*. 2008;4:129–38.
25. Li J, Wu S-T. Extended Cauchy equations for the refractive indices of liquid crystals. *J Appl Phys*. 2004;95:896–901.
26. Wu S-T. Design of a liquid crystal based tunable electrooptic filter. *Appl Opt*. 1989;28:48–52.
27. Mori H, Itoh Y, Nishiura Y, Nakamura T, Shinagawa Y. Performance of a novel optical compensation film based on negative birefringence of discotic compound for wide-viewing-angle twisted-nematic liquid-crystal displays. *Jpn J Appl Phys*. 1997;36:143–7.

## AUTHOR BIOGRAPHIES



**Jianghao Xiong** received his BS degree in Physics and BE in Computer Science and Technology from University of Science and Technology of China (USTC) and is currently working toward a PhD degree at the College of Optics and Photonics, University of Central Florida. His research interests include AR/VR displays, novel liquid crystal devices, holographic optical elements, and light field displays.



**Yannanqi Li** received her BS degree in Optics from Sichuan University in 2018 and is currently working toward a PhD degree at the College of Optics and Photonics, University of Central Florida. Her current research interests include novel liquid crystal optical elements, display system design, and new liquid crystal materials.

**Kun Li** received her PhD degree in Electrical Engineering from University of California at Berkeley in 2016 and is currently an optics engineering manager at Goertek, a leading high-tech manufacturer in acoustics, electronics, and optics. At Goertek optoelectronics, Dr Li's work focuses on design and manufacturing of optical components and modules for augmented reality (AR) near-eye display systems.



**Shin-Tson Wu** is Pegasus professor at the College of Optics and Photonics, University of Central Florida. He is among the first six inductees of the Florida Inventors Hall of Fame (2014) and a Charter Fellow of the National Academy of Inventors (2012). He is a fellow of the IEEE, OSA, SID, and SPIE, and an honorary professor at Nanjing University (2013) and at National Chiao Tung University (2018). He is the recipient of 2014 OSA Esther Hoffman Beller Medal, 2011 SID Slottow-Owaki Prize, 2010 OSA Joseph Fraunhofer Award, 2008 SPIE G. G. Stokes Award, and 2008 SID Jan Rajchman Prize.

**How to cite this article:** Xiong J, Li Y, Li K, Wu S-T. Aberration-free pupil steering Maxwellian display with wide-view broadband polarization converters. *J Soc Inf Display*. 2021;29:298–304. <https://doi.org/10.1002/jsid.1010>